Chinese Chemical Letters 31 (2020) 846–850

Contents lists available at ScienceDirect

Chinese Chemical Letters

journal homepage: www.elsevier.com/locate/cclet

Communication

TiC/C core/shell nanowires arrays as advanced anode of sodium ion batteries

Yanbin Shen[a], Yahao Li[a], Shengjue Deng[a], Guoxiang Pan[b], Qinqin Xiong[c], Xiaokun Ding[d], Yangfan Lu[a], Qi Liu[e], Xinhui Xia[a,f,*], Xiuli Wang[a], Jiangping Tu[a,*]

[a] State Key Laboratory of Silicon Materials, Key Laboratory of Advanced Materials and Applications for Batteries of Zhejiang Province, and School of Materials Science and Engineering, Zhejiang University, Hangzhou 310027, China
[b] Department of Materials Chemistry, Huzhou University, Huzhou 313000, China
[c] College of Materials and Environmental Engineering, Hangzhou Dianzi University, Hangzhou 310018, China
[d] Department of Chemistry, Zhejiang University, Hangzhou 310027, China
[e] Department of Physics, City University of Hong Kong, Hong Kong 999077, China
[f] Key Laboratory of Advanced Energy Materials Chemistry (Ministry of Education), College of Chemistry, Nankai University, Tianjin 300071, China

ARTICLE INFO

Article history:
Received 23 May 2019
Received in revised form 19 June 2019
Accepted 20 June 2019
Available online 24 June 2019

Keywords:
Sodium ion batteries
Nanowires
Core/shell structure
Carbon
Titanium carbide

ABSTRACT

High-performance anodes of sodium ion batteries (SIBs) largely depends on rational architecture design and binder-free smart hybridization. Herein, we report TiC/C core/shell nanowires arrays prepared by a one-step chemical vapor deposition (CVD) method and apply it as the anode of SIBs for the first time. The conductive TiC core is intimately decorated with carbon shell. The as-obtained TiC/C nanowires are homogeneously grown on the substrate and show core/shell heterostructure and porous architecture with high electronic conductivity and reinforced stability. Owing to these merits, the TiC/C electrode displays good rate performance and outstanding cycling performance with a capacity of 135.3 mAh/g at 0.1 A/g and superior capacity retention of 90.14% after 1000 cycles at 2 A/g. The reported strategy would provide a promising way to construct binder-free arrays electrodes for sodium ion storage.

It is crucial to develop green, low-cost and sustainable technologies for energy storage and conversion to meet the rapidly increasing demand of renewable energy source and drive the sustainable development of society [1–5]. Electrochemical energy including batteries and capacitors have attracted great attention owing to their high efficiency, excellent applicability, long cyclic lifetime and low environmental pollution [6–10]. At this stage, lithium ion batteries (LIBs) have become one of the most important energy storage systems and been widely used in portable electronic devices and automotive vehicles [11–15]. However, considering its high cost and unbalanced source distribution, it suffers from serious challenge for large-scale application. As sodium possesses similar chemical properties to lithium and the earth-abundant characteristic makes it very cost-effective, sodium ion batteries (SIBs) is thus regarded as one of the most promising alternatives to state-of-the-art LIBs [16–18]. However, it is not practical to directly utilize commercial graphite anodes for SIBs owing to the larger radius of Na^+ compared to Li^+, leading to low capacity and sluggish ion diffusion kinetics [19–21]. Therefore, hunting for alternative high-performance anode materials has become more significant on the research of SIBs.

Various materials including organic compounds [22], inorganic intercalation compounds [23], metal oxides [24,25], alloying metals [26] and carbon materials [27–29] have been developed as potential anode materials for SIBs. Typically, carbon materials stand out for its diversity of morphologies and structures, low cost and environment benign. Different kinds of carbon materials, including carbon nanotubes [30], hard carbon [31], graphene [29], carbon nanofibers [32], carbon nanowires [33] and porous carbons [34], have been reported as anode of SIBs. However, although most of these carbonaceous materials show good rate capability, their cycling performance is often not good enough as a result of huge volume changes during repeated cycles or unstable structures. For example, Nagalakshmi *et al.* [35] prepared mesoporous bio-carbon *via* the carbonization of cashew nut sheath and followed by KOH activation at different temperatures. The mesoporous bio-carbon exhibited good rate performance but unpleasant cyclic performance with the

* Corresponding authors at: State Key Laboratory of Silicon Materials, Key Laboratory of Advanced Materials and Applications for Batteries of Zhejiang Province, and School of Materials Science and Engineering, Zhejiang University, Hangzhou 310027, China.
E-mail addresses: helloxxh@zju.edu.cn (X. Xia), tujp@zju.edu.cn (J. Tu).

https://doi.org/10.1016/j.cclet.2019.06.044
1001-8417/

capacity retention dropped to 78.12% only after 100 cycles at 0.1 A/g. This phenomenon is quite common in such porous carbon materials, and to solve this issue, introducing a stable substrate or backbone for the growth of carbon is one of the most optimal options.

Recently, transition metal carbides (TMCs) have also been widely investigated as hard and anticorrosion coatings, machine parts and cutting tool components owing to their superior chemical stability, high melting point, high hardness and good electrical conductivity [36,37]. Among various TMCs, titanium carbide (TiC) has drawn more attention by virtue of its unique features including low density (4.93 g/cm^3), outstanding resistance to chemical attack and good electrical conductivity (6.8×10^{-5} Ω cm) [38]. Though TiC is an electrochemically inactive material in sodium-ion cells, both theoretical and experimental results demonstrate that TiC presents the strongest electrochemical stability as the support for active materials [39–42]. It has been confirmed that core/shell hybrid nanowires architecture cannot only offer rapid electron transfer and short ion diffusion channel, but also buffer great volume change and avoid fast capacity decay during long-term discharge-charge process especially at high rates. In view of the merits of well-defined geometry, good electrical conductivity and high electrochemical stability, TiC nanowires should also possess great potentials as the support for carbon materials as anodes of SIBs, to the best of our knowledge, has rarely been reported.

In this work, we reported a one-step CVD approach on the Ti_6Al_4V substrate to synthesize TiC/C core/shell nanowires arrays and their sodium ion storage performance as anode of SIBs is explored for the first time. The resulting TiC/C electrode displays good rate performance and outstanding cyclic performance with a capacity of 135.3 mAh/g at 0.1 A/g and high capacity retention of 90.14% after 1000 cycles at 2 A/g, which can be ascribed to the improved electron/ion transfer, high conductivity and stable core/shell structure. Our rational construction method opens up a new avenue for designing advanced anode materials for SIBs.

The TiC/C core/shell nanowires arrays are successfully synthesized on the Ti_6Al_4V substrate by a modified one-step CVD method. Scanning electron microscope (SEM) measurements were carried out to observe the appearance and morphology of the as-prepared sample. As shown in Figs. 1a and b , a great deal of *quasi*-vertical TiC/C nanowires with diameters of 300–500 nm are homogeneously grown on the substrate and leave numerous space between nanowires. Moreover, the surface of TiC/C nanowire is not smooth and kind of rough (Fig. 1c). The specific surface area was performed by Brunauer-Emmett-Teller (BET) analysis (Fig. S1 in Supporting information), which shows that the TiC/C nanowires has a specific surface area of about 41.1 m^2/g. The core/shell structure of TiC/C nanowire is obviously confirmed by transmission electron microscopy (TEM) images (Figs. 1d and e). The single crystallinity of the TiC core is proven by selected area electron diffraction (SAED) image (inset image in Fig. 1e), in which the diffraction spots are well indexed with the (111), (200) and (311) planes of TiC, respectively. The high-resolution TEM image of TiC/C (Fig. 1f) shows that the adjacent lattice spacing is around 0.22 nm, which is consistent with (200) planes of cubic TiC (JCPDS No. 65-8805), further supporting the formation of the single crystalline TiC core in the as-obtained core/shell material. Furthermore, the SAED image of the shell (Fig. 1g) shows no diffraction pattern, indicating that the TiC core is well covered by the amorphous carbon shell. In addition, the energy-dispersive spectroscopy (EDS) element mapping (Fig. 1h) not only shows the uniform distribution of Ti and C, but also further verifies the core/shell structure of the as-obtained TiC/C nanowire.

In order to study the crystal structure and phase composition of the as-prepared product, X-ray diffraction (XRD), Raman spectroscopy and X-ray photoelectron spectroscopy (XPS) were carried out. Fig. 2a depicts the XRD pattern of the TiC/C arrays and the diffraction peaks at 36.1°, 41.9°, 60.8°, 72.8° and 76.7° match well with the planes of (111), (200), (220), (311) and (222) of TiC (JCPDS No. 65-8805), respectively, while the peaks for carbon and Ti_6Al_4V substrate are also observed, again proving the successful preparation of TiC/C core/shell arrays. As for the Raman spectra of TiC/C (Fig. 2b), the strong peaks at 1346 and 1593 cm^{-1} belong to the D

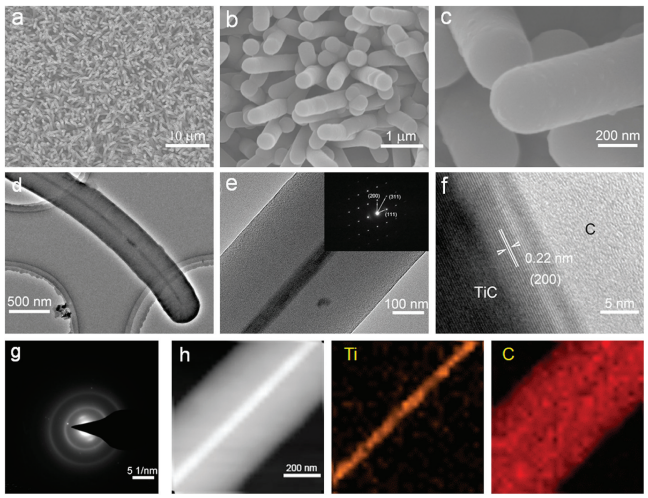

Fig. 1. (a–c) SEM images of TiC/C nanowires arrays. (d-f) TEM-HRTEM images of individual TiC/C nanowire (SAED pattern in inset). (g) SAED pattern of carbon shell in the heterostructure. (h) EDS mapping images of Ti and C in TiC/C heterostructure.

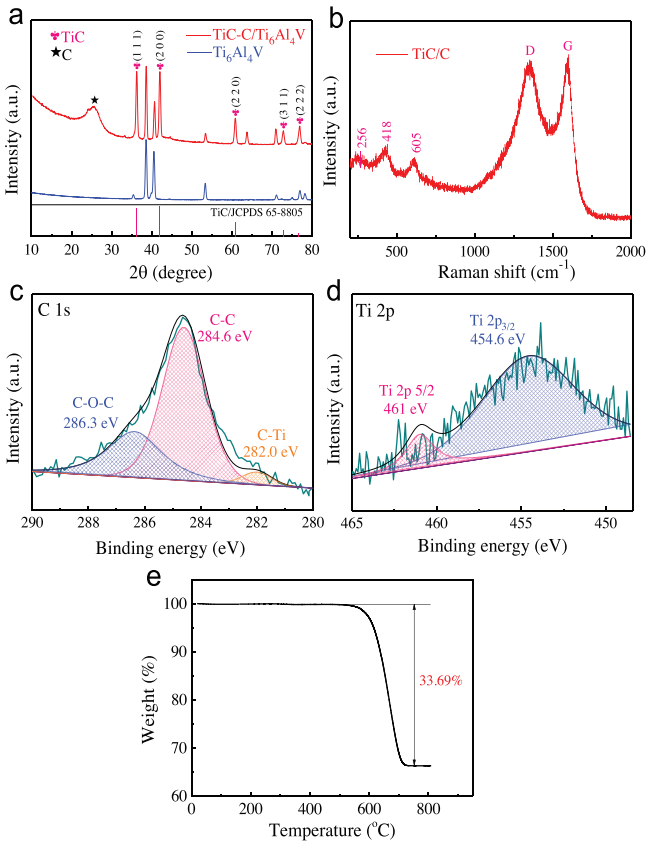

Fig. 2. Structural and composition characterization of TiC/C nanowire arrays. (a) XRD; (b) Raman spectra; (c,d) XPS spectra of C 1s and Ti 2p; (e) TGA curve under air atmosphere at a heating rate of 10 °C/min.

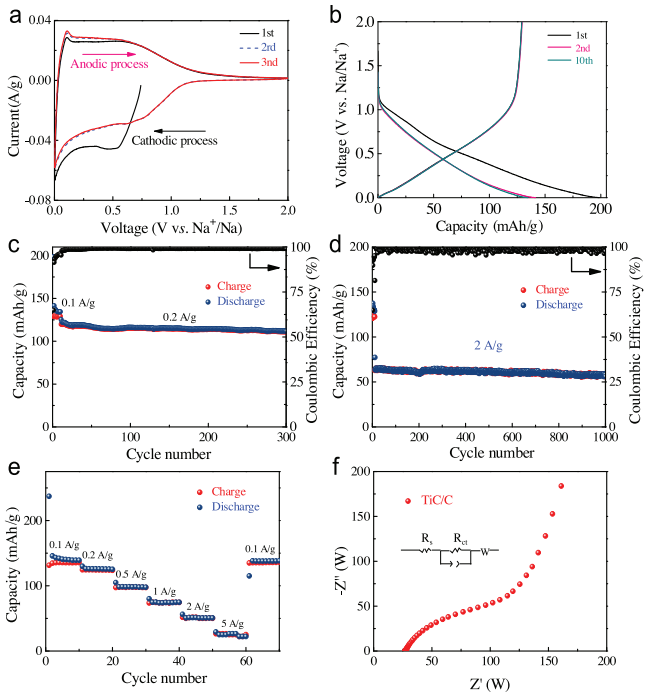

Fig. 3. Electrochemical performance characterization of TiC/C electrode for SIBs. (a) CV curves at a scan rate of 0.1 mV/s; (b) Charge-discharge curves at the current density of 0.1 A/g; (c, d) Cycling stability at 0.2 A/g and 2 A/g, respectively. (e) Rate performance. (f) Nyquist plots (the equivalent circuit model in inset).

band and G band of carbon, respectively, and the other peaks at 256, 418 and 605 cm^{-1} are ascribed to the characteristic peaks of TiC. XPS spectra of TiC/C hybrids are shown in Figs. 2c and d. The high-resolution spectra of C 1s (Fig. 2c) show two main peaks at 284.6 eV and 286.3 eV indexed well to C—C and C—O—C bond, respectively. As the TiC is well covered by C shell, the peak at 282.0 eV corresponding to the C—Ti bond is relatively weaker [40,43,44]. In the high-resolution Ti 2p XPS spectra (Fig. 2d), two peaks with the bonding energy of 461.0 eV and 454.6 eV are monitored, assigned to Ti $2p_{5/2}$ and Ti $2p_{3/2}$ peaks, respectively. All these results mutually support each other and suggest the successful fabrication of TiC/C nanowires arrays.

To characterize the sodium ion storage properties of the as-obtained TiC/C core/shell arrays, a series of electrochemical tests were carried out at room temperature. The capacity is calculated only based on the mass of carbon, which is determined by TGA (Fig. 2e). Fig. 3a shows the CV curves of TiC/C core/shell electrode within the voltage window of 0.01-3 V *vs.* Na/Na^+ at a scan rate of 0.1 mV/s. The reduction peak at 0.50 V is observed in the first cycle and disappears during the subsequent discharge process, which is corresponding to the formation of a solid electrolyte interface (SEI) layer derived from the decomposition of electrolyte and responsible for the large irreversible capacity loss during the first discharge-charge process. In the meanwhile, there is a cathodic peak at around 0.01 V and an anodic peak at 0.10 V in the curves, which are assigned to Na^+ insertion/desertion in the interlayer of carbon material, respectively. Then Fig. 3b depicts the discharge-charge profiles of TiC/C electrode at the current density of 0.1 A/g. An extended potential plateau at about 0.5 V appears in the first discharge curve and subsequently disappears, which is in good agreement with the CV results. The initial discharge capacity of the TiC/C reaches a capacity of 198.8 mAh/g and the relevant charge capacity is 135.3 mAh/g, showing an initial coulombic efficiency of 68.06%, higher than most of carbon materials owing to its unique core/shell structure and high conductivity (Table 1). The irreversible capacity in the first cycle primarily results from the formation of SEI layer and a few side reactions happening on the surface of the electrode. The follow-up curves almost overlap with each other, which indicates the excellent cyclic stability and reversibility of TiC/C electrode during the repeated discharge-charge process.

After the as-prepared electrode was activated at 100 mA/g for ten cycles, the cyclic performance and coulombic efficiency were measured at both 0.2 A/g and 2 A/g. As seen from Fig. 3c, the coulombic efficiency of TiC/C core/shell arrays electrode reaches 98% after activation and even exceeds 99% in the following cycles, indicating superior stability and reversibility. More importantly, as shown in Table 1, the TiC/C electrode demonstrates much better cyclic stability than other carbon materials. Its capacity only slightly decays from 125.4 mAh/g to 111.8 mAh/g after 300 cycles at 0.2 A/g (89.15% capacity retention based on the electrochemical process after activation). Moreover, the TiC/C electrode retains 90.14% of its initial capacity after activation even after charge and discharge of 2 A/g for 1000 cycles (Fig. 3d). In other words, the average capacity fading of TiC/C electrode for each cycle is small than 0.01%, which further suggests its merits over other carbon materials. The excellent capacity retention of the TiC/C core/shell nanostructure electrode can be attributed to its novel architecture and highly porous structure. Firstly, the voids among TiC/C nanowires can offer enough space to mitigate and accommodate the volume change. Secondly, the TiC nanowires have superior

Table 1
Comparison of carbon-based anodes reported in the literature for SIBs.

Materials	Precursor	Initial CE	Current density (A/g)	Capacity retention	References
TiC/C nanowires arrays	/	68.06%	0.2	89.15% (300 cycles)	This work
	/		2	90.14% (1000 cycles)	This work
Hard carbon	Apple waste	61%	1	85% (1000 cycles)	[45]
Porous carbons	Peanut skin	34%	0.5	86% (200 cycles)	[46]
Carbon nanosheets	Peat Moss	57.50%	0.2	85.57% (200 cycles)	[47]
Carbon sheets	Wheat straw	50.53%	1	55.62% (1400 cycles)	[48]
Carbon nanoparticles	Coconut oil	49%	0.1	73.28% (50 cycles)	[49]
Mesoporous carbon	Cashewnut sheath	/	0.1	78.12% (100 cycles)	[35]
rGO/CNTS	/	42.70%	0.05	61.46% (200 cycles)	[50]
Hollow carbon nanosphere	/	19.70%	0.1	72.46% (100 cycles)	[51]
Boron-doped 3D porous carbon	/	16%	0.1	60% (100 cycles)	[52]
Hard carbon	Subbituminous coal	79.50%	0.05	82% (150 cycles)	[53]
N-doped carbons	/	58%	0.1	62.31% (100 cycles)	[54]
porous carbon	/	82.40%	0.02	72.5% (100 cycles)	[55]
Hard carbon	reed straw	77.03%	0.12	86.7% (200 cycles)	[56]
Carbon fibers	/	32.12%	0.1	83.02% (100 cycles)	[57]
N-doped carbon nanofibers	/	29.30%	0.2	88.7% (200 cycles)	[58]
Carbon nanosheets	corncobs	30.96%	0.1	85.8% (200 cycles)	[59]

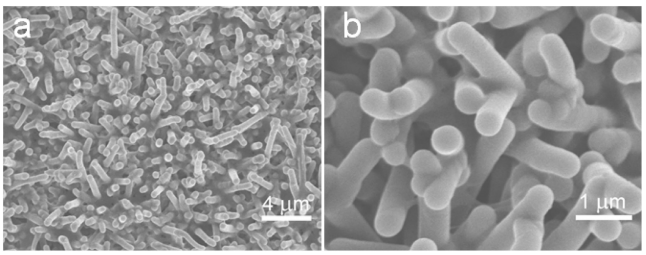

Fig. 4. SEM images of TiC/C nanowires arrays after 100 cycles at 2 A/g. Scale bar: 4 μm (a), 1 μm (b).

electrochemical and chemical stability, maintaining the nanowire structure integrity well during the repeated discharge-charge process.

Further, to study the high rate properties of TiC/C anode material, rate capability test was conducted at different current densities (increasing from 0.1 A/g to 5 A/g and eventually returning to 0.1 A/g). The TiC/C electrode delivers specific capacities of 135.3, 124.3, 97.7, 74.5, 50.8 and 25.1 mAh/g at 0.1, 0.2, 0.5, 1, 2 and 5 A/g, respectively (Fig. 3e). Even after experiencing severe charge-discharge condition, the capacity could be restored when the charge-discharge current density switches back to 0.1 A/g, suggesting the good rate performance of TiC/C electrode. SEM images of the electrode after 100 cycles were also obtained (Figs. 4a and b). It is clear that the electrode structure remains intact after cycling, further verifying the robustness of the TiC/C core/shell arrays, which lead to the excellent long-term stability and rate performance. Moreover, the superior structure stability of TiC/C anode is also supported by Raman analysis after cycling (Fig. S2 in Supporting information). Obviously, the characteristic peaks of carbon and TiC could be observed for the TiC/C sample, suggesting the excellent long-term stability by the synergistic advantages of TiC skeleton and carbon layer.

The corresponding charge transfer kinetics of the composite were further investigated by the electrochemical impedance spectroscopy (EIS) analysis (Fig. 3f). Nyquist plots comprise a straight sloping line in the low-frequency zone and a depressed semicircle in the high-frequency zone. The fitting of the Nyquist plots was also carried out and the obtained equivalent circuit is shown in the inset of Fig. 3f. The values of R_s, R_{ct} and W in the equivalent circuit model, reflect the total ohmic resistance of the electrode and the electrolyte, the electrochemical reaction resistance and the diffusion resistance of sodium ion, respectively. The sloping line in the low-frequency zone is related to the Na^+ diffusion kinetics, while the semicircle in the high-frequency zone represents the charge transfer resistance in the electrochemical reaction. The TiC/C electrode shows a low-frequency line with large slope, indicating high Na-ion diffusion coefficient in the electrode. Meanwhile, the radius of the depressed semicircle in the high-frequency zone is about 63 Ω, demonstrating relatively low charge-transfer resistance. The fairly small R_{ct} confirms the fast electron/ion transport on the electrode/electrolyte interface, which can be ascribe to the increased electrolyte/electrode contact area due to the core/shell nanostructure and the superior electrical conductivity of TiC core.

In conclusion, high-performance TiC/C core/shell nanowire arrays anode for SIBs has been successfully prepared *via* a facile CVD method on the Ti_6Al_4V substrate. The as-obtained TiC/C nanowire arrays possess core/shell nanostructure and porous architecture, providing increased accessible contact and active areas, excellent buffering ability for the volume change and fast electron/ion transfer. As a result, the TiC/C electrode exhibits good rate performance, extraordinary cycling performance with a high capacity retention of 89.15% after 300 cycles at 0.2 A/g and a superior long-term cyclability with 90.14% capacity retention after 1000 cycles at 2 A/g. The developed electrode strategy can provide reference for fabrication of other binder-free arrays materials for SIBs.

Acknowledgments

This work is supported by the National Natural Science Foundation of China (Nos. 51772272 and 51728204), Fundamental Research Funds for the Central Universities (No. 2018QNA4011), Qianjiang Talents Plan D (No. QJD1602029), Startup Foundation for Hundred-Talent Program of Zhejiang University and Analysis Testing and Commonweal Project of Zhejiang Province (No. GC19E020005). The authors acknowledge the TEM support from Qiaohong He and Xiaokun Ding and SEM support from Fang Chen from Department of Chemistry, Zhejiang University.

Appendix A. Supplementary data

Supplementary material related to this article can be found, in the online version, at doi:https://doi.org/10.1016/j.cclet.2019.06.044.

References

[1] F. Zhao, X. Zhao, B. Peng, et al., Chin. Chem. Lett. 29 (2018) 1692–1697.
[2] A.J. Hu, S. Jin, Z.Z. Du, H.C. Jin, H.X. Ji, J. Energy Chem. 27 (2018) 203–208.
[3] J. Yang, X. Xiao, P. Chen, et al., Nano Energy 58 (2019) 455–465.
[4] J. Yan, Q. Wang, T. Wei, Z.J. Fan, Adv. Energy Mater. 4 (2014) 1300816.
[5] S. Shen, X. Xia, Y. Zhong, et al., Adv. Mater. 31 (2019) 1900009.
[6] Y. Zhong, X.H. Xia, S.J. Deng, et al., Adv. Mater. 30 (2018) 1805165.
[7] Y. Chen, B. Wang, T. Hou, et al., Chin. Chem. Lett. 29 (2018) 187–190.
[8] L. Zhang, Y. Ding, J. Song, Chin. Chem. Lett. 29 (2018) 1773–1776.
[9] Y. Han, Y. Lu, S. Shen, et al., Adv. Funct. Mater. 29 (2019) 1806329.
[10] R. Wang, Y. Han, Z. Wang, et al., Adv. Funct. Mater. 28 (2018) 1802157.
[11] S. Shen, S. Deng, Y. Zhong, et al., Chin. Chem. Lett. 28 (2017) 2219–2222.
[12] X.H. Xia, S.J. Deng, S.S. Feng, J.B. Wu, J.P. Tu, J. Mater. Chem. A 5 (2017) 21134–21139.
[13] D.D. Shan, J. Yang, W. Liu, J. Yan, Z.J. Fan, J. Mater. Chem. A 4 (2016) 13589–13602.
[14] Q. Xiong, C. Zheng, H. Chi, J. Zhang, Z. Ji, Nanotechnology 28 (2017) 055405.
[15] Q.Q. Xiong, J.J. Lou, X.J. Teng, et al., J. Alloys Compd. 743 (2018) 377–382.
[16] Z. Zhao, Y. Ye, W. Zhu, et al., Chin. Chem. Lett. 29 (2018) 629–632.
[17] W. Li, R. Fang, Y. Xia, et al., Batteries Supercaps (2018) 1800067.
[18] L. Yang, W. Wang, M.X. Hu, J.J. Shao, R.T. Lv, J. Energy Chem. 27 (2018) 1439–1445.
[19] L. Xiao, H. Lu, Y. Fang, et al., Adv. Energy Mater. 8 (2018) 1703238.
[20] J. Zhan, S. Deng, Y. Zhong, et al., Nano Energy 44 (2018) 265–271.
[21] X. Xia, S. Deng, D. Xie, et al., J. Mater. Chem. A 6 (2018) 15546–15552.
[22] X. Wang, C. Zhang, Y. Xu, et al., Macromol. Chem. Phys. 219 (2018) 1700524.
[23] Q.Q. Yang, M.C. Liu, Y.M. Hu, et al., J. Energy Chem. 27 (2018) 1208–1213.
[24] A.S. Etman, J. Sun, R. Younesi, J. Energy Chem. 30 (2019) 145–151.
[25] X.H. Xia, S.J. Deng, D. Xie, et al., J. Mater. Chem. A 6 (2018) 15546–15552.
[26] J.S. Choi, H.J. Lee, J.K. Ha, K.K. Cho, J. Nanosci. Nanotechnol. 18 (2018) 6459–6462.
[27] L. Zhang, X. Xia, Y. Zhong, et al., Adv. Mater. 30 (2018) 1804011.
[28] Y. Zhong, X. Xia, J. Zhan, X. Wang, J. Tu, J. Mater. Chem. A 4 (2016) 11207–11213.
[29] Y. Zhang, X. Xia, B. Liu, et al., Adv. Energy Mater. 9 (2019) 1803342.
[30] K. Wang, Y. Huang, X. Qin, et al., Chem. Eng. J. 317 (2017) 793–799.
[31] E. Demir, M. Aydin, A.A. Arie, R. Demir-Cakan, J. Alloys Compd. 788 (2019) 1093–1102.
[32] P.Y. Zhao, J. Zhang, Q. Li, C.Y. Wang, J. Power Sources 334 (2016) 170–178.
[33] Y. Cao, L. Xiao, M.L. Sushko, et al., Nano Lett. 12 (2012) 3783–3787.
[34] H.g. Wang, Z. Wu, F.l. Meng, et al., Chemsuschem 6 (2013) 56–60.
[35] M. Nagalakshmi, N. Kalaiselvi, Electrochim. Acta 304 (2019) 175–183.
[36] X. Xia, J. Zhan, Y. Zhong, et al., Small 13 (2017) 1602742.
[37] Y. Zhong, X. Xia, F. Shi, et al., Adv. Sci. 3 (2016) 1500286.
[38] Z.J. Yao, X.H. Xia, D. Xie, et al., Adv. Funct. Mater. 28 (2018) 1802756.
[39] H. Chun-Hsien, G. Dong, Z. Dongyuan, D. Ruey-An, Chem. Mater. 22 (2010) 1760–1767.
[40] S. Deng, F. Yang, Q. Zhang, et al., Adv. Mater. 30 (2018) 1802223.
[41] L. Hu, K. Huo, R. Chen, et al., Chem. Commun. 46 (2010) 6828–6830.
[42] S. Cao, Z. Xue, C. Yang, et al., Nano Energy 50 (2018) 25–34.
[43] X.H. Xia, Y.Q. Zhang, D.L. Chao, et al., Energy Environ. Sci. 8 (2015) 1559–1568.
[44] X. Yuan, L. Cheng, L. Kong, X. Yin, L. Zhang, J. Alloys Compd. 596 (2014) 132–139.
[45] L. Wu, D. Buchholz, C. Vaalma, G.A. Giffin, S. Passerini, ChemElectroChem 3 (2016) 292–298.
[46] H. Wang, W. Yu, J. Shi, et al., Electrochim. Acta 188 (2016) 103–110.
[47] J. Ding, H. Wang, Z. Li, et al., ACS Nano 7 (2013) 11004–11015.

[48] D. Qin, S. Chen, J. Solid State Electrochem. 21 (2016) 1305–1312.
[49] R.R. Gaddam, D. Yang, R. Narayan, et al., Nano Energy 26 (2016) 346–352.
[50] J. Feng, L. Dong, X. Li, et al., Electrochim. Acta 302 (2019) 65–70.
[51] K. Zhang, X. Li, J. Liang, et al., Electrochim. Acta 155 (2015) 174–182.
[52] D. Wang, Z. Wang, Y. Li, et al., Appl. Surf. Sci. 464 (2019) 422–428.
[53] H. Lu, S. Sun, L. Xiao, et al., ACS Appl. Energy Mater. 2 (2019) 729–735.
[54] W. Alkarmo, F. Ouhib, A. Aqil, et al., Macromol. Rapid Commun. 40 (2019) 1800545.
[55] G.X. Pan, F. Cao, D. Xie, Y.J. Zhang, X.H. Xia, Electrochim. Acta 292 (2018) 935–941.
[56] Z. Yao, X. Xia, Y. Zhang, et al., Nano Energy 54 (2018) 304–312.
[57] D. Flores, J. Villarreal, J. Lopez, M. Alcoutlabi, Mater. Sci. Eng. B 236 (2018) 70–75.
[58] Z. Wang, L. Qie, L. Yuan, et al., Carbon 55 (2013) 328–334.
[59] Q. Jiang, Z. Zhang, S. Yin, et al., Appl. Surf. Sci. 379 (2016) 73–82.